Deformation Compensation during Buoyancy-Enabled Inkjet Printing of 3D Soft Tubular Structures

Kyle Christensen[1], Zhengyi Zhang[2], Changxue Xu[3], Yong Huang[1,4]*

[1]Department of Mechanical and Aerospace Engineering, University of Florida, Gainesville, FL 32611, USA

[2]School of Naval Architecture and Ocean Engineering, Huazhong University of Science and Technology, Wuhan 430074, PR China

[3]Department of Industrial, Manufacturing, and Systems Engineering, Texas Tech University, Lubbock, TX 79409, USA

[4]Department of Biomedical Engineering, University of Florida, Gainesville, FL 32611, USA

*Corresponding author, Department of Mechanical and Aerospace Engineering, University of Florida, Gainesville, FL 32611, USA, Phone: 001-352-392-5520, Fax: 001- 352-392-7303, Email: yongh@ufl.edu

Abstract:

Of various tissues being fabricated using bioprinting, three-dimensional (3D) soft tubular structures have often been the focus since they address the need for printable vasculature throughout a thick tissue and offer potential as perfusable platforms for biological studies. Drop-on-demand inkjetting has been favored as an effective technique to print such 3D soft tubular structures from various hydrogel bioinks. During the buoyancy-enabled inkjet fabrication of hydrogel-based soft tubular structures, they remain submerged in a solution which crosslinks the printed structures and provides a supporting buoyant force. However, because of the low stiffness of the structures, the structural deformation of printed tubes poses a significant

challenge to the process effectiveness and efficiency. To overcome this structural deformation during buoyancy-enabled inkjet printing, predictive compensation approaches are developed to incorporate deformation allowance into the designed shape. Circumferential deformation is addressed by a four-zone approach which includes base, circular, vertical, and spanning zones for the determination of a designed cross section or compensated printing path. Axial deformation is addressed by the modification of the proposed circumferential compensation based on the distance of a given cross section to the junction of a branching tube. These approaches are found to enable the successful fabrication of straight and branching alginate tubular structures with nearly ideal geometry, providing a good foundation for the wide implementation of the buoyancy-enabled inkjetting technique. While inkjetting is studied herein as a model bioprinting process, the resulting knowledge also applies to other buoyancy-enabled bioprinting techniques.

Keywords: Bioprinting, structural deformation, deformation compensation, tubular structure

Nomenclature

v_{fp}	Feature printing velocity
v_{nfp}	Non-feature printing velocity
R_1	Undeformed radius of curvature
R_2	Deformed radius of curvature
ω	Change in radii of curvature
θ	Angular position

M	Applied moment
ν	Poisson's ratio
E	Young's modulus
t	Tube wall thickness
R	Designed tube radius
$L_x(\theta)$	*x*-direction distance between the centers of subsequent adjacent layers
h_v	Height of vertical zone
$h_{spanning}$	Height of spanning zone
$N_{spanning}$	Number of layers in the spanning zone
N	Layer number within the spanning zone
h_N	Height of each printed layer
$x_{circumferential}(\theta)$	*x*-direction location of the center of layers in the spanning zone
C_1, C_2	Constants defining designed cross section of the spanning zone
$x_{axial}(\theta, l)$	*x*-direction location of the center of layers in the axial compensation zone
l	Axial distance measured from a junction
$C_3(l)$	Constant defining designed cross section of axial compensation zone
X_{max}	Maximum displacement compensation value

L_b	Length of significant bowing deformation
Ro	Roundness
W	Width ratio
D_i	Diameter of maximum inscribed circle
D_c	Diameter of minimum circumscribed circle
W_j	Tube width at innermost cross section at junction

1. Introduction

Bioprinting, the layer-by-layer additive manufacturing of living tissues, has emerged as a promising approach to address the critical need for implantable human organs [1, 2]. Generally, it can be implemented using droplet-based approaches such as inkjet [3-7] and laser printing [8, 9], as well as filament-based approaches such as microextrusion [10, 11] and filament/rod assembly [12, 13]. In addition, printed tissue constructs offer countless opportunities as platforms for biomedical research including elucidating diseased tissue behavior and drug treatment effects [14].

While bioprinting offers a great promise for various biomedical applications, difficulty in printing anatomically relevant geometries still hinders progress toward the fabrication of living tissues. In particular, the printing of vascularized thick tissues is a grand challenge faced by the research community. Since adequate vascularization is required throughout a living tissue for the regulation of nutrients and waste, the fabrication of vascular or vascular-like constructs is often identified as the first step toward successful organ printing. Various fabrication techniques utilizing fugitive inks/sacrificial materials followed by cell seeding [15-17] were pioneered to facilitate the fabrication of vascularized cellular structures. However, living cells were usually

either seeded or uniformly cast instead of being directly printed, lacking much needed precise control of cellular heterogeneity throughout structures. Fortunately, bioprinting, with droplet-based techniques in particular, offers potential for the freeform fabrication of three dimensional (3D) heterogeneous cellular structures where the precise number and location of various cell types can be controlled with micrometer resolution, and therefore are favored over those which require cell seeding or casting for many thick tissue fabrication applications.

Vasculature within a thick tissue extends three-dimensionally throughout. Therefore, the ability to print both vertical and horizontal tubular structures as a basic building block is critical for the freeform fabrication of vascular systems. Because of the low stiffness of printed vascular or vascular-like structures, they easily experience structural deformation during fabrication [6, 7]. Specifically, the deformation of tube walls into or away from the lumen resulting in a noncircular cross section has been reported [6] despite the presence of a supporting solution. To enable the fabrication of tubular structures, the structural deformation during 3D bioprinting should be addressed.

The objective of this study is to investigate an empirical method instead of a purely heuristic approach to compensate for printing-induced structural deformation during the fabrication of alginate-based soft tubular structures. Compensation approaches are implemented to modify the designed geometry of structures, i.e. the locations of printed layers, such that the effects of deformation are alleviated. These approaches are developed and refined empirically based on experimental observations. Deformation is classified as circumferential or axial for tubular structures, and the resulting knowledge may be applied to compensate for similar structural deformation of soft structures with lumens, overhangs, and spanning features during 3D bioprinting. Since inkjet printing has been widely implemented for the fabrication of

biological structures and offers good resolution, scalability, and high cell viability [3-7], and there may be undesirable structural deformation during printing [6, 7, 18], it is studied herein as a model bioprinting technique. While buoyancy-enabled inkjet printing is investigated in this study, the proposed compensation approach is also applicable for other droplet-based as well as filament-based bioprinting techniques.

2. Background

Defects and deformation are very typical during additive manufacturing/3D printing because of its layer-by-layer fabrication nature. Defects and deformation include surface artifacts such as a staircase surface appearance due to the formation of parts from discrete layers [19] and the loss of macroscopic dimensional accuracy of printed parts. To address the defect and deformation issue during printing, numerous studies [20-25] have been devoted to mitigating various discrepancies between designed and resulting part geometries. Unlike surface appearance imperfections, unwanted variation in part dimensions cannot typically be rectified through the optimization of printing conditions alone. The occurrence of these dimensional discrepancies is greatly dependent on part geometry and the mechanism for material deposition and solidification, and in most cases is due to shrinkage, expansion, and warpage of printed materials. As such, printing with predictive or predefined deformation/shrinkage compensation has been an effective approach to mitigate such deformation during various printing processes including stereolithography (SLA), fused deposition modeling, and binder jetting, to name a few. Firstly, shrinkage and warpage are two very common defects because of the temperature sensitivity and phase change of build materials and/or the nonuniformity of printed structures, and they can be mitigated accordingly. Unwanted part shrinkage has been reported using SLA,

and has been corrected for by developing shrinkage functions and a compensation model to enable preemptive modification of the computer-aided design (CAD) model [24]. A similar approach has been reported by modifying the CAD model to counteract the anisotropic or nonuniform shrinkage and warping effects during the fused deposition of ceramics [21]. Shrinkage and warping of parts created by binder jetting has also been reported, and pre-deformation of the part geometry using freeform deformation [20] has been utilized to counteract these effects [25]. Secondly, dimensional accuracy of printed parts has been of concern too, and this can be overcome accordingly. Print-through occurring during SLA has been shown to form larger-than-designed layers, and researchers have compensated for this inconsistency by decreasing the designed layer thickness using analytical relations between process parameters and resulting geometry [22]. Binder jetting has also been shown to create larger-than-expected layers due to binder bleeding, which has been corrected for by decreasing the amount of binder deposited [23].

Of aforementioned studies [20-25], the goal has been to preemptively compensate for the mechanism causing dimensional inaccuracy by modifying the designed part geometry before printing, such that an ideal geometry results after shrinkage, expansion, or warpage. These structures [20-25] are usually stiff in nature, which is different from soft tubular structures fabricated using bioprinting. When bioprinting tubular structures, the main defect/deformation is the structural deformation because of the limited stiffness of biomaterials such as hydrogels. Although the structural deformation is not attributed to shrinkage, expansion, and warpage, a heuristic predictive compensation approach has been successfully implemented to mitigate such structural deformation during buoyancy-enabled inkjet printing [6, 18]. The general heuristic approach for the development of deformation compensation which enables the fabrication of

nearly ideal geometries using inkjet bioprinting can be summarized as follows: a structure is first printed with a designed cross section that is identical to the ideal resulting cross section. Process-induced deformation is characterized and the mechanisms to counteract that deformation are considered. The printing paths which determine the designed cross section are then modified to compensate for the deformation, and the structure is printed with a new designed cross section. The resulting cross section is again characterized and the process of modifying the designed cross-sectional shape followed by observing the resulting shape is iterated. The process continues until the resulting cross section is acceptably representative of the ideal cross section. As such, the designed shape of tubular structures is systematically modified through iterative experiments such that an ideal geometry results after deformation.

While the heuristic approach for deformation compensation can be effective, there is a need for a systematic approach for effective printing of soft tubular structures. As with approaches for other additive manufacturing processes [20-25], it is ideal to implement analytical model-based predictive compensation considering heat transfer, solid mechanics, fluid mechanics, etc. Unfortunately, as observed, deformation of printed structures is found to accumulate throughout the printing process due to the deposition of layers and the low stiffness of hydrogel-based tubular structures. While a great deal is understood about this deformation process, thus far analytical models cannot readily be applied to predict this deformation because of the continuously-changing geometry during printing and the unknown gelation state and resulting stiffness of printed structures over time. As such, the development of a realizable systematic approach to achieve acceptable tubular geometries using inkjet bioprinting is of great importance.

3. Deformation during Buoyancy-Enabled Inkjet Printing of Soft Tubular Structures

A representative buoyancy-enabled inkjet bioprinting approach [18] as illustrated in Fig. 1 is implemented as a model bioprinting system herein to study the aforementioned deformation compensation problem. Bioink droplets are generated by a nozzle-based inkjet printhead mounted to a set of linear computerized *xy* stages. The printhead deposits droplets continuously at a specified frequency while the *xy* stages control its movement along designed printing paths: at a feature printing velocity v_{fp} for the deposition of layers, and a much faster non-feature printing velocity v_{nfp} when traversing zones where material buildup is undesirable [18], such as across the lumen of a tubular structure. The receiving substrate is mounted to an independent linear *z* stage. Sequentially, deposited droplets coalesce to form a layer on the top of a previous layer. After a new layer is deposited, the platform substrate is lowered into the crosslinking and supporting dual-purpose solution by the designed thickness of the layer. This solution acts to both gel each printed layer and support the structure during printing. The printing process continues layer-by-layer in a typical additive manufacturing approach until a 3D structure is complete.

Typical vascular-like structures include horizontal and vertical components. Figure 2 illustrates the formation process of a new layer during the buoyancy-enabled inkjet bioprinting of horizontal tubular structures, which are more challenging to print than vertical tubular structures since they are subject to structural deformation because of their universal spanning features. Structures printed with a designed circular cross section have been shown to consistently result in deformed tear drop-shaped cross sections [6]. During printing, the most recently deposited layer is observed to remain at the surface of the supporting solution (Fig. 2(a)) because of the surface tension effect. When a new layer is deposited, the previously printed layer is displaced

downward by the thickness of the newly deposited layer (Fig. 2(b)). The platform substrate is then lowered by the layer thickness, which effectively stretches the printed structure upward mainly because of buoyancy and surface tension effects (Fig. 2(c)). Due to the combined effect of buoyance, surface tension and gravity on a not well-supported soft structure, the structural deformation of horizontal tubes is inevitable during buoyancy-enabled inkjet bioprinting, resulting in the variation between designed and resulting cross sections. The final shape is the result of deformation occurring throughout the printing process due to the deposition of each layer as illustrated in Fig. 2. Herein, the term "designed cross section" refers to the printing path or the physical location of layers to be printed based on the computerized motion control of an inkjet printhead.

For vascular-like structures with horizontal and vertical tubular features, both features may experience different types of deformation during buoyancy-enabled inkjet bioprinting. Generally, soft vertical tubular structures may experience buckling, collapse, and imbalance during printing [5], which are not strictly related to structural deformation and should be mitigated by design and material selection instead. For soft horizontal tubular structures, structural deformation due to overhangs and spanning features across the lumen [7] may be identified and mitigated by process planning, so such structural deformation is selected for research in this study.

Structural deformation of horizontal tubular structures may be classified as either circumferential (Fig. 3(a)) or axial, where axial (or axially-varying [7]) deformation varies for the fabrication of straight (Fig. 3(b)) or branching (Fig. 3(c)) tubes. Circumferential (or hoop) deformation (Fig. 3(a)) is defined as the formation of a tear drop-shaped cross section [6] because of excessive bending, despite a circular cross section as designed. Axial deformation

(Fig. 3(b) and (c)) is defined as the variation in circumferential deformation occurring along the longitudinal axis of a tube. For straight tubes, the resulting cross-sectional width is increased toward the center producing a barreled appearance, despite a uniform cross section along its axis as designed. For branching tubes, deformation varies along the longitudinal axis, resulting in increased width (as a bowing shape) close to the branching junction [7]. Both circumferential and axial deformation problems are addressed herein, and corresponding compensation approaches are detailed which enable the fabrication of horizontal tubular structures with nearly ideal cross sections. While this study presents compensation approaches for the fabrication of horizontal tubular structures, the resulting knowledge may also be applied to other 3D features.

4. Deformation Analysis and Compensation Approach

4.1. Compensation of circumferential deformation

The circumferential deformation of horizontal tubes can be modeled by considering an infinitesimally thin slab from a tube, and its deflection is approximated as the deflection of a curved beam as shown in Fig. 4. Center lines of initial (undeformed) and deformed tubular structures are represented by dashed and solid lines, and their radii of curvatures are denoted by R_1 and R_2, respectively. There is a difference ω between the two radii, which is a function of angular position θ. The entire cross section may be considered as two symmetrical curved beams, so the governing equation for structural deformation under an applied moment M can be written as follows while Equation (2) is the alternative expression of Equation (1):

$$\frac{1}{R_2}-\frac{1}{R_1}=\frac{12(1-\nu^2)MR_1^2}{Et^3} \tag{1}$$

$$\frac{d^2\omega}{d\theta^2}+\omega=\frac{12(1-\nu^2)MR_1^2}{Et^3} \tag{2}$$

where ν is the Poisson's ratio, E is the Young's modulus, and t is the wall thickness. The main forces acting on the curved beams are composed of the droplet impact force, buoyant force due to the supporting solution, and weight. Based on the moment resulting from each force, the governing equation for the deformation of a curved beam can be further established. Equations (1) and (2) are presented as a step toward analytically modeling deformation which may occur during inkjet bioprinting. However, it is difficult to solve such a governing equation since the material properties (E and ν) are largely unknown and vary throughout printing as gelation occurs over time.

For a more straightforward implementation, a four-zone compensation method is proposed and discussed herein. Four zones have been identified within the designed cross section based on the unique mode of deformation observed within each zone. Empirical approaches are used to modify $L_x(\theta)$, the x-direction distance between the centers of two subsequent layers, in each zone to compensate for this deformation. These zones are: base zone (Fig. 5(a)), circular zone (Fig. 5(b)), vertical zone (Fig. 5(c)), and spanning zone (Fig. 5(d)), and are found to be sufficient for printing horizontal tubes with resulting circular cross sections. While deformation modeling using Equations (1) and (2) provides insight into the implementation of deformation compensation and may be utilized in future studies, a simplified empirical implementation approach is favored herein.

For the fabrication of the base zone, the bottom part of the cross section, inconsistencies in the tube wall are compensated for by reducing L_x. If a circular interpolation is chosen for the printing of lower parts of the cross section, L_x may be too large for the deposited layers to be effectively connected as shown in the inset of Fig. 5(a) because of the very small tangential slope. For example, a circular interpolation of a 3 mm diameter tube with a layer height of 0.05

mm leads to a maximum L_x of 550 μm in the base zone. A large distance such as this between any two adjacent layers is found to result in weakened zones or even gaps in the tube wall. Thus, additional layers should be included in this zone to mitigate the problem due to large L_x. The maximum allowable L_x is chosen as the droplet diameter (~120 μm herein) to ensure the connectivity between adjacent layers. For adjacent layers which have L_x larger than this, an additional layer is printed at the midpoint of these two layers. Material deposition rates, and thus layer heights, for these three layers are adjusted accordingly to prevent overprinting while still maintaining a coherent base.

For the fabrication of the circular zone, a circular interpolation is used to determine layer positions. It is found experimentally that no significant deformation occurs during the fabrication of this circular zone up until the midpoint of the cross section, i.e. the structure height equals the tube radius. The transition from the base zone to the circular zone occurs at the onset of sufficiently small L_x when using a circular interpolation such that the inclusion of an additional layer is no longer needed. In this study, the circular zone begins once a circular interpolation provides a maximum L_x comparable to the printed droplet diameter (~120 μm).

The printing path for the vertical and spanning zones is determined simultaneously. There is a spanning zone in which L_x is increased to account for the increasing deformation when layers are deposited over the lumen space, resulting in very few deposited layers [6] and thus a reduced overall height. To compensate for this reduced height, a vertical zone is proposed where several layers are deposited with $L_x = 0$ to increase the overall height of the cross section. An initial height for the vertical zone is chosen as $R/2$ for a designed tube radius R, and then the printing path for the subsequently printed spanning zone is determined as discussed in the following paragraph. Once the printing path for the spanning zone is determined, the height of the vertical

zone h_v is further estimated by subtracting the height of the spanning zone $h_{spanning}$ from the tube radius as shown in Equation (3):

$$h_v(R) = R - h_{spanning}(R) \tag{3}$$

where $h_{spanning}$ is estimated as follows:

$$h_{spanning}(R) = \sum_{N=1}^{N_{spanning}} h_N \tag{4}$$

where $N_{spanning}$ is the total number of layers in the spanning zone and can be determined experimentally, N is the layer number within the spanning zone (1 for the first printed layer, 2 for the second printed layer, etc.), and h_N is the height of each layer as designed. Both the height of the vertical zone and printing path for the spanning zone are then optimized experimentally. Despite layers within the vertical zone being deposited vertically, they are found to deform inward to form a curved region in the final cross section after the spanning zone is printed.

For the fabrication of the spanning zone, the location of each deposited layer is modified by increasing L_x proportionately to account for increasing deformation. Inward bending deformation in the x direction resulting from each deposited layer is extremely high during the fabrication of the uppermost zone of the cross section, the spanning zone. This may be attributed to the relatively large arc length of the tubular cross section and the increased rotational moment at the layer deposition location. If fabricating a tube with a circular designed cross section and no compensation, the drastic increase in x-direction deformation leads to an undesirable tear drop-shaped cross section as shown in Fig. 3(a). To achieve a circular cross section, an empirical approach is taken in which Equation (5) is used to determine $x_{circumferential}(\theta)$, the x-direction location of the center of each printed layer within the spanning zone as measured from the cross-

sectional center, based on the tube radius R and experimentally determined constants C_1, C_2, and N ($N \in [1, N_{spanning}]$):

$$x_{circumferential}(\theta) = R \pm (C_1 N)^{C_2} \tag{5}$$

Equation (5) is implemented as a straightforward means to modify the designed cross-sectional shape. An exponential curve was determined experimentally to adequately compensate for deformation occurring within the spanning zone by increasing L_x to account for increasing deformation. C_1 and C_2 define the curve forming the cross section and are modified to increase L_x at an appropriate rate while spanning the tube radius. The increased L_x results in fewer layers being deposited to span the gap across the top of the tube. This decreases the overall height of the structure, where the height of the spanning zone $h_{spanning}$ is determined by Equation (4), and the resulting height decrease is remedied by the inclusion of the previously described vertical zone.

4.2. Compensation of axial deformation

4.2.1. Description of axial deformation

Axial deformation, also called axially-varying deformation [7], describes the variation in the degree of circumferential deformation along the longitudinal axis of tubes and usually occurs in two cases: tubes with increased length are found to result in wider cross sections toward the center as shown in Fig. 3(b), and tubes with a branching feature are found to result in wider cross sections toward the junction as shown in Fig. 3(c). In both cases, this is attributed to a variation in local effective stiffness, or the resistance to inward bending deformation, along the longitudinal axis of structures.

For a given wall thickness, the effects of circumferential deformation of straight tubes are uniform throughout for relatively low aspect ratio tubes, such as tubes with a 1 mm wall thickness, 3 mm diameter, and 5 mm length. However, for higher aspect ratio tubes such as tubes with a 1 mm wall thickness, 3 mm diameter, and 10 mm length, the degree of circumferential deformation varies along the longitudinal tube axis as shown in Fig. 3(b). That is, circumferential deformation increases the resulting width more toward the center of the tube, resulting in a nonuniform diameter along the axial direction.

As described previously, the inward bending deformation of the tube walls during the deposition of the spanning zone plays a key role in the resulting cross section. For a given material, the degree of this inward bending deformation is dependent on the local effective stiffness. As illustrated in Fig. 6(a) and (b), the effective stiffness of a partially complete tubular structure varies along its longitudinal axis. That is, an inward bending force applied at the tube open ends results in a larger deformation than a counterpart force applied to other regions of the tube. This is attributed to the variation in the volume of material contributing to the energy of deformation along the tube axis. The less-constrained tube open end experiences a larger deformation and deforms a smaller volume of material compared to that at other locations. It is somewhat analogous to the application of a force at the end of a cantilever compared to the center or other locations of a simply supported beam. As such, a smaller inward bending deformation and thus a larger width occurs toward the center of a completed straight tube, in particular with large aspect ratio tubes as shown in Fig. 3(b).

During the fabrication of horizontal branching structures, the overall resulting tube is bowed outward with increasing severity toward the branching junction because of the variation in local effective stiffness. As mentioned previously, the control of wall deformation during the

deposition of the upper half of tubular structures (the spanning zone, in particular) is key to the formation of a circular cross section. As with axial deformation of straight tubes, the magnitude of the inward bending deformation is dependent on the local effective stiffness of structures, which is found to vary along the longitudinal axes too. Furthermore, the tube walls resisting inward bending deformation at a junction are no longer perpendicular to the direction of deformation, leading to an increased effective stiffness as illustrated in Fig. 6(b). This increased local stiffness in turn leads to resulting branching structures with an increased width toward the junction.

Generally, axial deformation of high aspect ratio straight tubes is highly dependent on the wall thickness of structures and the material properties such as the Young's modulus, and its effects may only be pronounced with thin-walled tubes. As such, this may be effectively mitigated by adopting a thicker tube wall instead of any structural compensation. However, axial deformation occurring in tubular structures with branching junctions is more severe and not easily remedied by increasing the wall thickness even though the wall thickness can be adjusted for some applications. Thus, a compensation approach is articulated below for branching tubes, while an approach for straight tubes is not particularly developed herein. It should be noted that a compensation approach for straight tubes without junctions may be considered as a special case of the proposed approach for branching structures.

4.2.2. Compensation of axial deformation of branching tubes

For deformation compensation of branching tubes, the proposed approach integrates the proposed circumferential compensation approach with additional modification of the designed geometry toward the junction. Logically, the increased resulting width of structures near a

junction due to deformation may be compensated for by decreasing the designed width of the cross section to a varying degree based on the proximity to a junction. Herein, Equation (6) is proposed to empirically reduce the designed width by modifying $x_{axial}(\theta,l)$, the *x*-direction location of the center of each printed layer within the axial compensation zone as measured from the cross-sectional center at any axial distance *l* from a junction. This equation provides an implementable guideline to modify the designed shape based on the tube radius *R* and a geometry modification constant $C_3(l)$, which is defined by Equation (7), where X_{max} is the maximum displacement compensation value and determined at the midpoint of a cross section at a junction ($l = 0$) for the experimentally-determined length of significant bowing deformation L_b as shown in Fig. 6 (c) and (d). The layer deposition location $x_{circumferential}$ at a given axial location is determined by the aforementioned four zone-based circumferential compensation approach.

$$x_{axial}(\theta,l) = \pm\left(\left|x_{circumferential}(\theta)\right| - C_3(l)\left[1-\left(\frac{R-\left|x_{circumferential}(\theta)\right|}{R}\right)^2\right]\right) \tag{6}$$

$$C_3(l) = \left(\frac{L_b - l}{L_b}\right)X_{max} \tag{7}$$

It can be seen that Equation (6) inherits the four-zone approach for circumferential compensation, but scales the *x*-direction deposition position along the longitudinal axis. For the cross section at a given axial location *l*, $C_3(l)$ defines the maximum innermost *x*-direction displacement which occurs at the vertical midpoint ($z = 0$) of the cross section. Equation (6) scales the *x*-direction inward bending displacement to take full effect at the vertical midpoint and no effect at the top ($z = R$) or bottom ($z = -R$) of the tube. As observed, the variation in resulting tube width is relatively linear with a maximum effect at a junction and minimal effect at the tube

open ends. As such, Equation (7) linearly scales the tube geometry modification based on the distance from a junction l to have full effect at the junction and no effect at a distance (L_b) from the junction where bowing deformation is no longer significant. It is noted that axial deformation of the layers of the base zone is not compensated for since circumferential compensation itself is already sufficient to achieve the designed geometry. This leads to the first layer of the circular zone being printed toward the inner side of the base zone as illustrated in Fig. 6(e) in order to reduce the tube width, but does not produce any discontinuities in the tube wall as observed.

5. Experimental Validation

5.1. Materials and experimental conditions

Alginate is a widely used hydrogel in biomedical research [26, 27], so sodium alginate (Sigma-Aldrich, St. Louis, MO) was selected as a model hydrogel to prepare the bioink solution in this study. The resulting alginate solution had a final concentration of 1% (w/v) in deionized (DI) water for the fabrication of acellular structures. While the inkjet bioprinting approach implemented herein is capable of fabricating viable cellular structures [7], only acellular bioink was used for the development of deformation compensation approaches. Structures were printed into a bath of 2% (w/v) calcium chloride (Sigma-Aldrich) prepared in DI water, which gelled sodium alginate droplets upon deposition due to the ionic crosslinking mechanism. In addition, the crosslinking solution provided a supporting buoyant force during fabrication. The densities of the resulting calcium alginate hydrogel and supporting solution were measured as 1.066 g/cm^3 and 1.007 g/cm^3, respectively. This near match in density indicates that the supporting buoyant force is substantial when compared to the gravitational force. Tensile testing of typical calcium

alginate revealed the Young's modulus on the order of 10 kPa [28], indicating that the hydrogel is relatively soft and susceptible to deformation.

Alginate bioink droplets were continuously generated by a 120 μm diameter piezoelectric inkjet printhead (MJ-ABL, MicroFab, Plano, TX) at a frequency of 60 Hz. Linear computerized *xyz* stages (Aerotech, Pittsburgh, PA) controlled motion between the printhead and receiving substrate. The feature printing velocity v_{fp} ranged from 150-300 mm/min for the deposition of layers and the non-feature printing velocity v_{nfp} was 600 mm/min. All tubular structures had a designed diameter of 3 mm and branching structures were designed with a long tube length of 10 mm and short tube length (symmetric) of 5 mm. The tube wall for each layer was deposited by a single travel of the printhead.

5.2. Circumferential compensation result

As reported previously [6], the fabrication of short horizontal tubular structures was achieved through iterative modification of designed shape such that printing-induced deformation was compensated for, achieving a circular cross section. Herein, a four-zone approach was implemented to achieve a circular cross section as designed. The locations of additional base layers were determined as previously described to ensure a coherent and well-connected base. For the circular zone, layer locations were based on a circular interpolation. The number of layers in the vertical zone was estimated based on the vertical zone height (Equation (3)) and determined to be 10. The compensated x position of each deposited layer was determined using Equation (4) with the experimentally-determined constants $C_1 = 1.75\times10^{-2}$ and $C_2 = 1.90$ for the spanning zone. Figure 7(a) shows a resulting cross section without any compensation, and the designed cross section or compensated printing path resulting from

circumferential compensation is plotted in Fig. 7(b). This modified cross section is found to enable the fabrication of horizontal tubular structures with a 3 mm diameter and 5 mm length with nearly ideal cross sections as illustrated in Fig. 7(c). For tubular structures with a relatively small aspect ratio (D=3 mm and length=5 mm) as shown in Fig. 7, only circumferential compensation is required to achieve a circular cross section throughout.

5.3 Integrated circumferential and axial compensation result

Both circumferential and axial compensation were implemented for the fabrication of a horizontal branching structure with uniform circular diameter throughout. The compensated x position of each layer within the cross section at the junction was determined using Equation (5), and deformation was found to be sufficiently alleviated with X_{max} = 0.6 mm. Axial deformation was found to be insignificant past a length of 5 mm from the junction after trial printing tests, so L_b was chosen as 5 mm. The designed cross section at the junction is shown in Fig. 8(a) with the deposition location of each layer indicated for the cross section at the junction (both circumferential and axial compensation). The projected printing paths for the final ten printed layers are plotted in Fig. 8(b), illustrating the linear variation in designed width from L_b to the junction. This designed cross section after compensation enabled the fabrication of horizontal branching tubular structures with a 3 mm diameter, 5 mm short branch length, and 10 mm long branch length with nearly ideal cross sections as shown in Fig. 9. For tubular structures with a branching junction and a relatively large aspect ratio (D=3 mm and length=10 mm) as shown in Fig. 9, both circumferential and axial compensation are required to achieve a circular cross section throughout.

5.4. Compensation evaluation metrics

The effectiveness of the proposed deformation compensation approaches is further quantified using the roundness *Ro* and a width ratio *W*. The International Organization for Standardization (ISO) defines a measure of roundness as the ratio between the diameters of the maximum inscribed circle D_i and minimum circumscribed circle D_c about a shape. This metric is used to quantify the roundness of horizontal tubular cross sections as shown in Fig. 10(a) and (b). It is found that roundness is improved from 0.79 to 0.92 by the incorporation of circumferential compensation for the structure as shown in Fig. 10(a). A width ratio *W* is defined to evaluate the axial deformation at the junction of branching structures as the tube width at the innermost cross section at the junction W_j divided by the designed width. The width ratio is evaluated for horizontal branching structures as shown in Fig. 10(c) and (d). The width ratio is found to improve from 1.61 to 1.08 by the incorporation of both circumferential and axial compensation approaches for the structure as shown in Fig. 10(c). Both of the metrics demonstrate the effectiveness of the proposed approaches for the compensation of structural deformation during buoyancy-enabled inkjet printing. While not directly measured, it is found that both circumferential and axial compensation approaches have enabled the fabrication of structures with relatively uniform wall thicknesses throughout and a final printed volume comparable to the ideal volume.

6. Conclusions and Future Work

In this study, deformation compensation approaches are developed to enable the fabrication of soft tubular structures, in particular, horizontal tubular structures with circular cross sections during buoyancy-enabled inkjet bioprinting. It is found that structures undergo

severe structural deformation during printing which results in noncircular cross sections and may be classified as circumferential or axial. Circumferential deformation occurs for tubular structures with relatively low aspect ratios and results in tear drop-shaped cross sections because of excessive bending. Axial deformation occurs for high aspect ratio or branching structures as the degree of circumferential deformation varies along the longitudinal axis of structures because of the variation in stiffness.

A four-zone compensation approach is proved to be effective in overcoming circumferential deformation, which includes empirical printing path planning for the proposed base, circular, vertical, and spanning zones within the designed cross section. Axial deformation is addressed by the modification of the proposed circumferential compensation based on the distance of a given cross section to the junction of a branching tube. The implementation of circumferential compensation has enabled the fabrication of horizontal straight tubes with circular cross sections, and branching structures with uniform circular cross sections throughout have been successfully fabricated by integrating the circumferential and axial compensation approaches.

Future work may aim to develop analytical models for the determination of deformation compensation with the inclusion of characterized mechanical properties of hydrogel structures. More generalized compensation approaches for a variety of geometries may be investigated. Additional comparisons between structures printed with and without compensation including the uniformity of wall thickness throughout, total printed volume, etc. may be conducted. The robustness of compensation approaches should be further assessed for a broad range of geometries, and complex 3D structures should be fabricated by incorporating improved compensation approaches.

Acknowledgement

This work was partially supported by the U.S. National Science Foundation (NSF CMMI-1634755).

References

[1] Ringeisen, B. R., Pirlo, R. K., Wu, P. K., Boland, T., Huang, Y., Sun, W., Hamid, Q., and Chrisey, D. B., 2013, "Cell and Organ Printing Turns 15: Diverse Research to Commercial Transitions," MRS Bulletin, **38**(10), pp. 834-843.

[2] Huang, Y., Leu, M. C., Mazumder, J., and Donmez, A., 2015, "Additive Manufacturing: Current State, Future Potential, Gaps and Needs, and Recommendations," ASME J. of Manufacturing Sci. and Eng., **137**(1), p. 014001.

[3] Boland, T., Tao, X., Damon, B. J., Manley, B., Kesari, P., Jalota, S., and Bhaduri, S., 2007, "Drop-On-Demand Printing of Cells and Materials for Designer Tissue Constructs," Mat. Sci. Eng. C, **27**(3), pp. 372–376.

[4] Nishiyama, Y., Nakamura, M., Henmi, C., Yamaguchi, K., Mochizuki, S., Nakagawa, H., and Takiura, K., 2009, "Development of a Three-Dimensional Bioprinter: Construction of Cell Supporting Structures Using Hydrogel and State-Of-The-Art Inkjet Technology," J. Biomech. Eng., **131**(3), p. 035001.

[5] Xu, C., Chai, W., Huang, Y., and Markwald, R. R., 2012, "Scaffold-Free Inkjet Printing of Three-Dimensional Zigzag Cellular Tubes," Biotechnol. Bioeng., **109**(12), pp. 3152–3160.

[6] Xu, C., Christensen, K., Zhang, Z., Huang, Y., Fu, J., and Markwald, R. R., 2013, "Predictive Compensation-Enabled Horizontal Inkjet Printing of Alginate Tubular Constructs," Manufacturing letters, **1**(1), pp. 28-32.

[7] Christensen, K., Xu, C., Chai, W., Zhang, Z., Fu, J., and Huang, Y., 2015, "Freeform Inkjet Printing of Cellular Structures with Bifurcations," Biotech. Bioeng., **112**(5), pp. 1047-1055.

[8] Yan, J., Huang, Y., and Chrisey, D. B., 2012, "Laser-Assisted Printing of Alginate Long Tubes and Annular Constructs," Biofabrication, **5**(1), p. 015002.

[9] Xiong, R., Zhang, Z., Chai, W., Huang, Y., and Chrisey, D. B., 2015, "Freeform Drop-On-Demand Laser Printing of 3D Alginate and Cellular Constructs," Biofabrication, **7**(4), p. 045011.

[10] Duan, B., Hockaday, L., Kang, K., and Butcher, J., 2013, "3D Bioprinting Heterogeneous Aortic Valve Conduits with Alginate/Gelatin Hydrogels," J. Biomed. Mater. Res. Part A, **101A**(5), pp. 1255-1264.

[11] Jin, Y., Compaan, A., Bhattacharjee, T., and Huang, Y., 2016, "Granular Gel Support-Enabled Extrusion of Three-Dimensional Alginate and Cellular Structures," Biofabrication, **8**(2), p. 025016.

[12] Norotte, C., Marga, F. S., Niklason, L. E., and Forgacs, G., 2009, "Scaffold-Free Vascular Tissue Engineering Using Bioprinting Biomaterials," **30**(30), pp. 5910-5917.

[13] Skardal, A., Zhang, J., and Prestwich, G. D., 2010, "Bioprinting Vessel-Like Constructs Using Hyaluronan Hydrogels Crosslinked with Tetrahedral Polyethylene Glycol Tetracrylates," Biomaterials, **31**(24), pp. 6173-6181.

[14] Murphy, S. V., and Atala, A., 2014, "3D Bioprinting of Tissues and Organs," Nature Biotechnology, **32**(8), pp. 773-785.

[15] Miller, J., Stevens, K., Yang, M., Baker, B., Nguyen, D., Cohen, D., Toro, E., Chen, A., Galie, P., Yu, X., Chaturvedi, R., Bhatia, S., and Chen, S., 2012, "Rapid Casting of Patterned

Vascular Networks for Perfusable Engineered Three-Dimensional Tissues," Nature materials, **11**(9), pp. 768-774.

[16] Kolesky, D. B., Truby, R. L., Gladman, A. S., Busbee, T. A., Homan, K. A., and Lewis, J. A., 2014, "3D Bioprinting of Vascularized, Heterogeneous Cell-Laden Tissue Constructs," Adv. Mater., **26**(19), pp. 3124-3130.

[17] Van Hoorick, J., Declercq, H., De Muynck, A., Houben, A., Van Hoorebeke, L., Cornelissen, R., Van Erps, J., Thienpont, H., Dubruel, P., and Van Vlierberghe, A., 2015, "Indirect Additive Manufacturing as an Elegant Tool for the Production Of Self-Supporting Low Density Gelatin Scaffolds," J. Mater. Sci. Mater. Med., **26**(10), p. 247.

[18] Xu, C., Zhang, Z., Christensen, K., Huang, Y., Fu, J., and Markwald, R. R., 2014, "Freeform Vertical and Horizontal Fabrication of Alginate-Based Vascular-Like Tubular Constructs Using Inkjetting," ASME J. of Manufacturing Sci. and Eng., **136**(6), p. 061020.

[19] Armillotta, A., 2006, "Assessment of Surface Quality on Textured FDM Prototypes," Rapid Prototyping Journal, **12**(1), pp. 35-41.

[20] Sederberg, T. W., and Parry, S. R., 1986, "Free-Form Deformation of Solid Geometric Models," SIGGRAPH Computer Graphics (ACM), **20**(4), pp. 151-160.

[21] McIntosh, J. J., Danforth, S. C., and Jamalabad, V. R., 1997, "Shrinkage and Deformation in Components Manufactured by Fused Deposition of Ceramics," *Proceedings of the Solid Freeform Fabrication Symposium*, University of Texas, Austin, pp. 159-166.

[22] Limaye, A. S., and Rosen, D. W., 2006, "Compensation Zone Approach to Avoid Print-Through Errors in Mask Projection Stereolithography Builds," Rapid Prototyping Journal, **12**(5), pp. 283-291.

[23] Stopp, S., Wolff, T., Irlinger, F., and Lueth, T., 2008, "A New Method for Printer Calibration and Contour Accuracy Manufacturing with 3D-Print Technology," Rapid Prototyping Journal, **14**(3), pp. 167-172.

[24] Huang, Q., Zhang, J., Sabbaghi, A., Dasgupta, T., and Epstein, D. J., 2015, "Optimal Offline Compensation of Shape Shrinkage for 3D Printing Processes," IIE Transactions, **47**(5), pp. 431-441.

[25] Schmutzler, C., Zimmermann, A., and Zaeh, M. F., 2015, "Compensating Warpage of 3D Printed Parts Using Free-Form Deformation," Procedia CIRP, **41**, pp. 1017-1022.

[26] Nakamura, M., Iwanaga, S., Henmi, C., Arai, K., and Nishiyama, Y., 2010, "Biomatrices and Biomaterials for Future Developments of Bioprinting and Biofabrication," Biofabrication, **2**(1), p. 014110.

[27] Sun, J., and Tan, H., 2013, "Alginate-Based Biomaterials for Regenerative Medicine," Materials, **6**(4), pp. 1285-1309.

[28] Jin, Y., Compaan, A., Bhattacharjee, T., and Huang, Y., 2016, "Granular Gel Support-Enabled Extrusion of Three-Dimensional Alginate and Cellular Structures," Biofabrication, **8**(2), p. 025016.

Deformation Compensation during Buoyancy-Enabled Inkjet Printing of 3D Soft Tubular Structures

Kyle Christensen, Zhengyi Zhang, Changxue Xu, Yong Huang

List of Figures

and (d) a spanning zone with large L_x to compensate for increased deformation occurring in this zone.

Fig. 6. (a) CAD design of a partially-complete horizontal branching structure, (b) illustration of the variation in resistance to inward bending deformation, or effective stiffness, along the longitudinal axis of the tube and at the junction, (c) and (d) resulting shape of a horizontal branching structure because of the variation in stiffness without and with compensation, respectively, and (e) illustration of axial compensation algorithm.

Fig. 7. (a) Deformed cross section of a horizontal tube without compensation, (b) designed cross section or compensated printing path with layer locations indicated in blue, and (c) resulting circular cross section after compensation.

Fig. 8. (a) Designed cross section or compensated printing path at the junction ($l = 0$) with layer locations indicated in blue after incorporating circumferential and axial deformation compensation, and (b) projected printing paths incorporating the proposed compensation approaches.

Fig. 9. Horizontal branching tubular structure printed after the incorporation of circumferential and axial deformation compensation (scale bars: 3 mm).

Fig. 10. Roundness R and width ratio W metrics for the evaluation of (a, b) circumferential compensation and (c, d) axial compensation results, respectively.

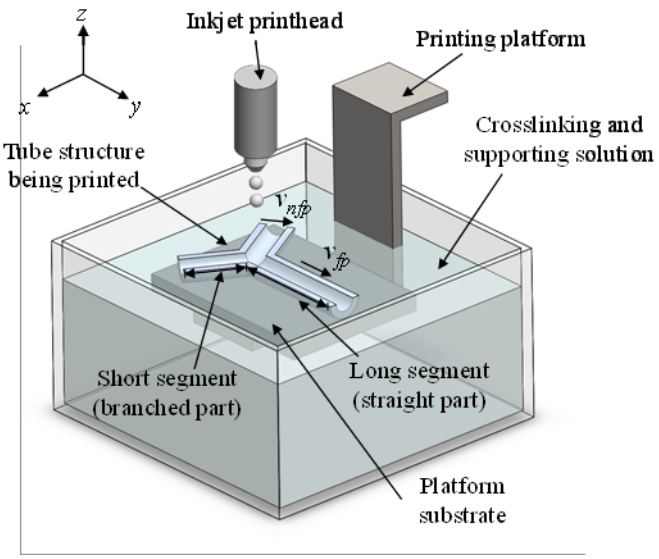

Fig. 1. Illustration of a representative buoyancy-enabled inkjet bioprinting approach.

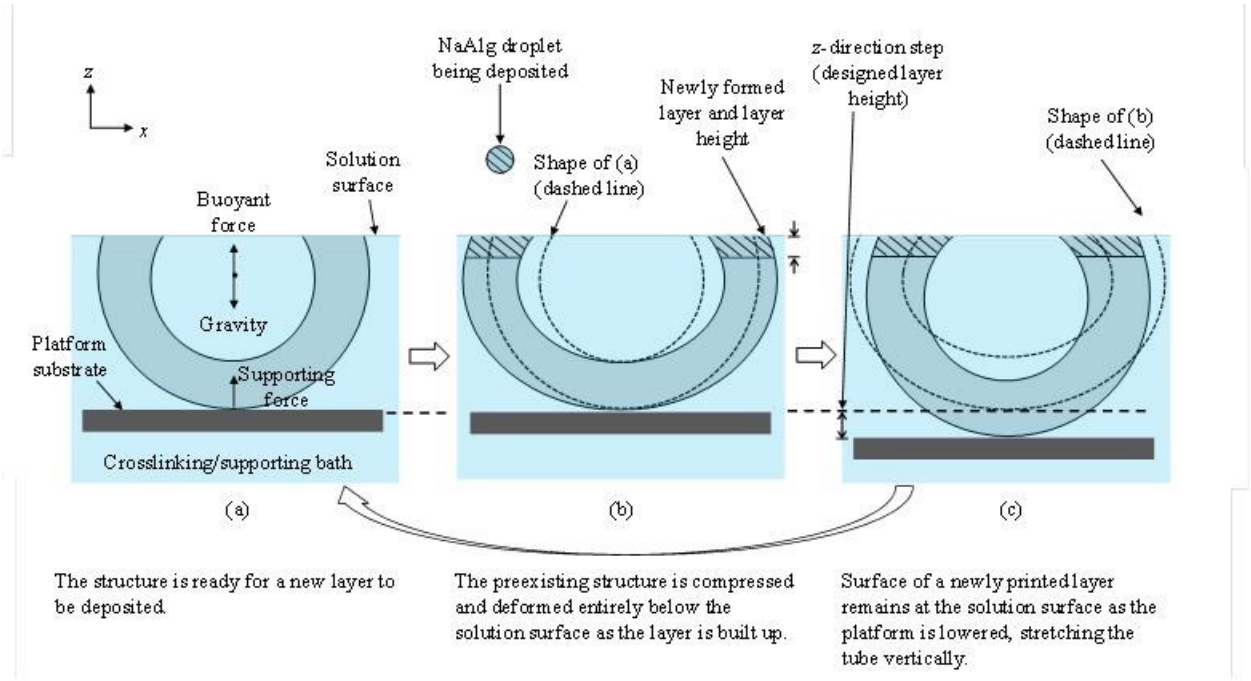

Fig. 2. Cross-sectional view of layer deposition. (a) Prior to layer deposition, the tube is supported by the buoyant force and remains at the solution surface because of the surface tension effect. (b) As a layer is printed, the preexisting structure deforms downward and is compressed beneath the surface. (c) The substrate is then lowered by the layer thickness, effectively stretching the structure vertically.

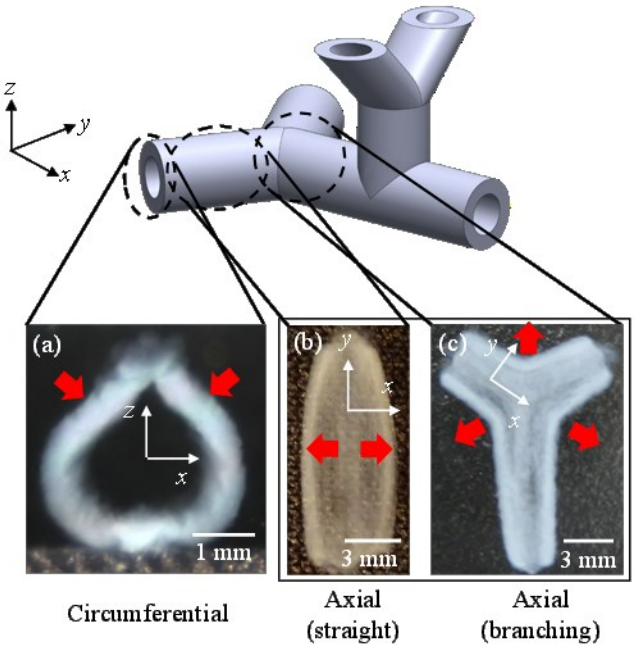

Fig. 3. Illustration of structural deformation types of horizontal tubes: (a) circumferential, (b) axial (straight tube), and (c) axial (branching tube) occurring during printing.

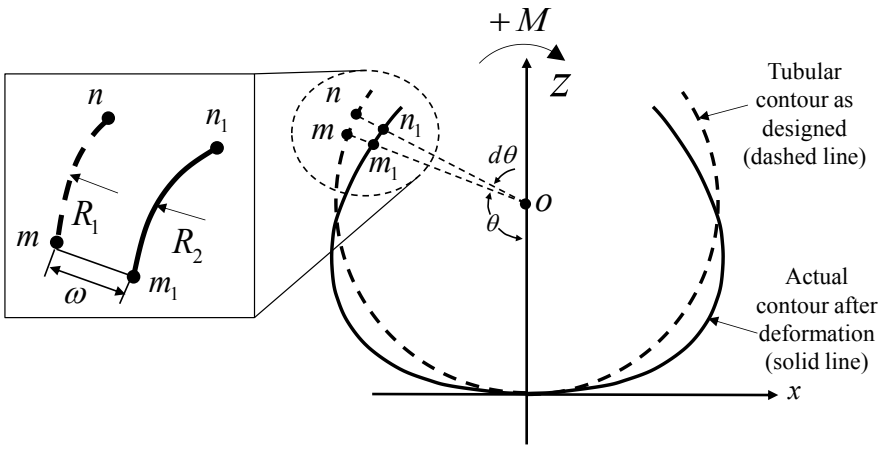

Fig. 4. Deflection of a curved beam representing the deformation of a tubular cross section during printing.

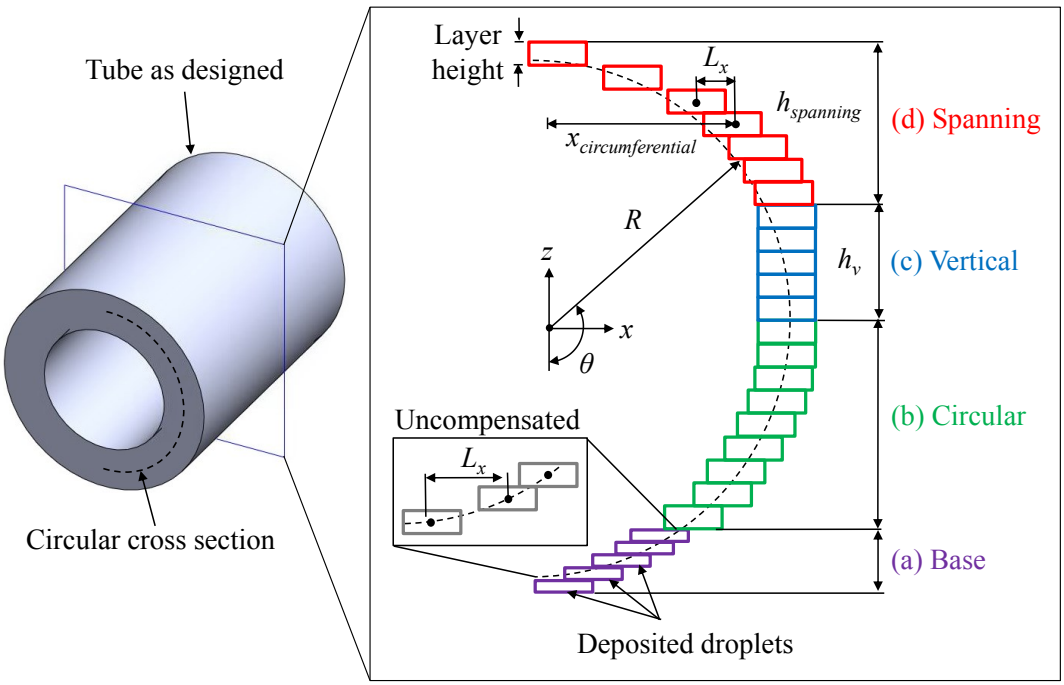

Fig. 5. Illustration of four distinct zones for deformation compensation: (a) a base zone with additional layers (small L_x) to prevent gaps in the structure. Uncompensated layer locations are shown inset with L_x defined as the x distance between the centers of two consecutive layers, (b) a circular zone as no substantial deformation is observed in this zone, (c) a vertical zone to increase the overall height of the tubular structure ($L_x = 0$), and (d) a spanning zone with large L_x to compensate for increased deformation occurring in this zone.

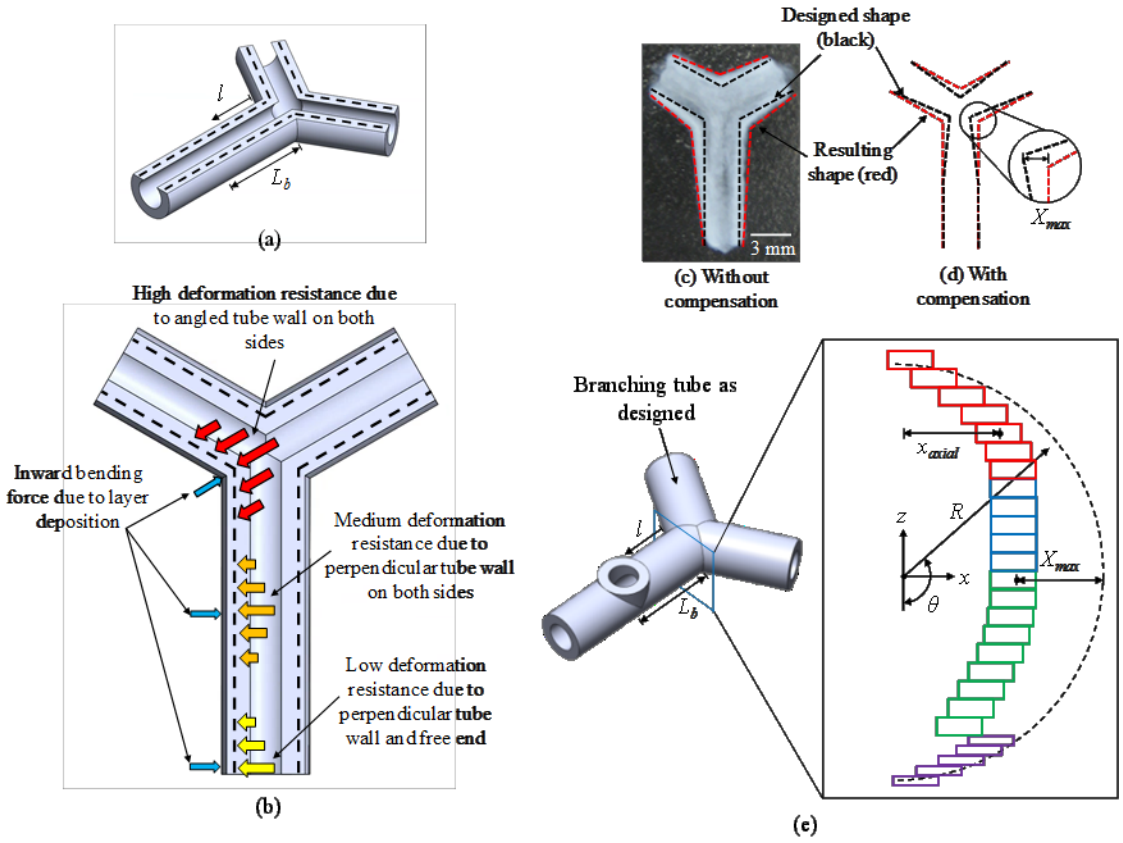

Fig. 6. (a) CAD design of a partially-complete horizontal branching structure, (b) illustration of the variation in resistance to inward bending deformation, or effective stiffness, along the longitudinal axis of the tube and at the junction, (c) and (d) resulting shape of a horizontal branching structure because of the variation in stiffness without and with compensation, respectively, and (e) illustration of axial compensation algorithm.

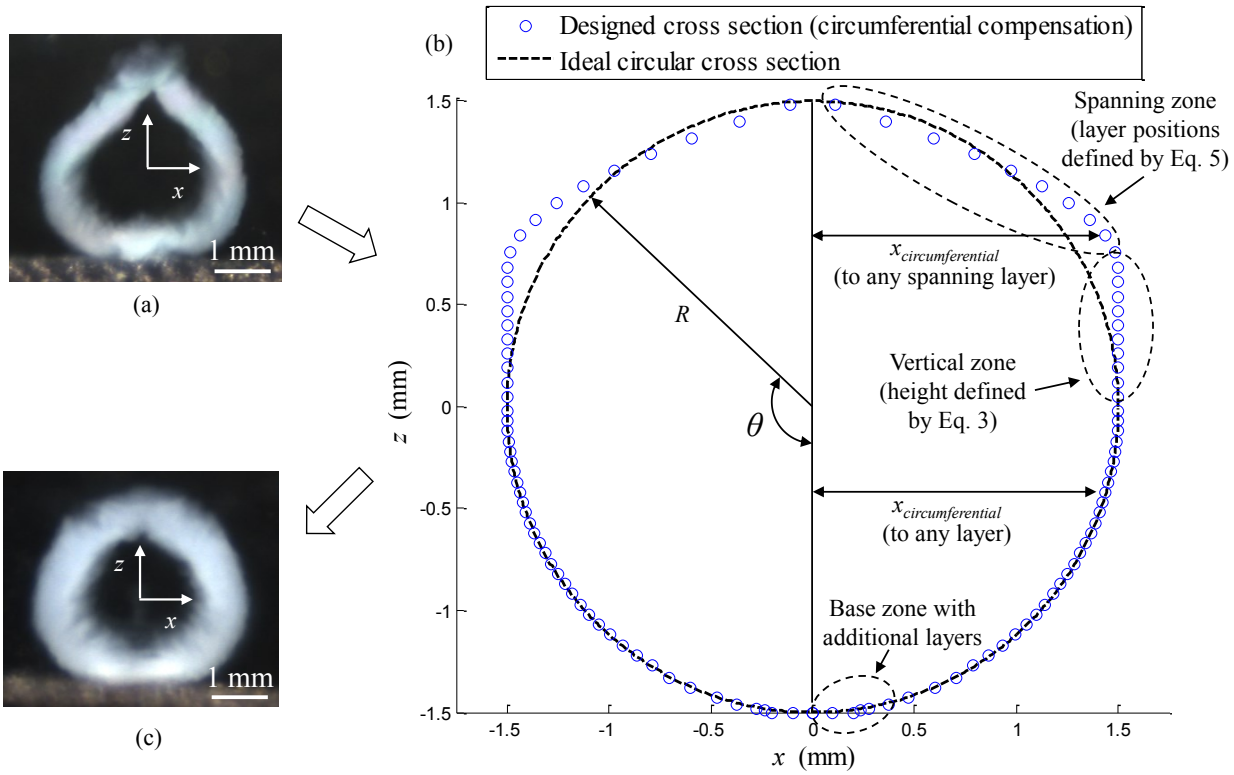

Fig. 7. (a) Deformed cross section of a horizontal tube without compensation, (b) designed cross section or compensated printing path with layer locations indicated in blue, and (c) resulting circular cross section after compensation.

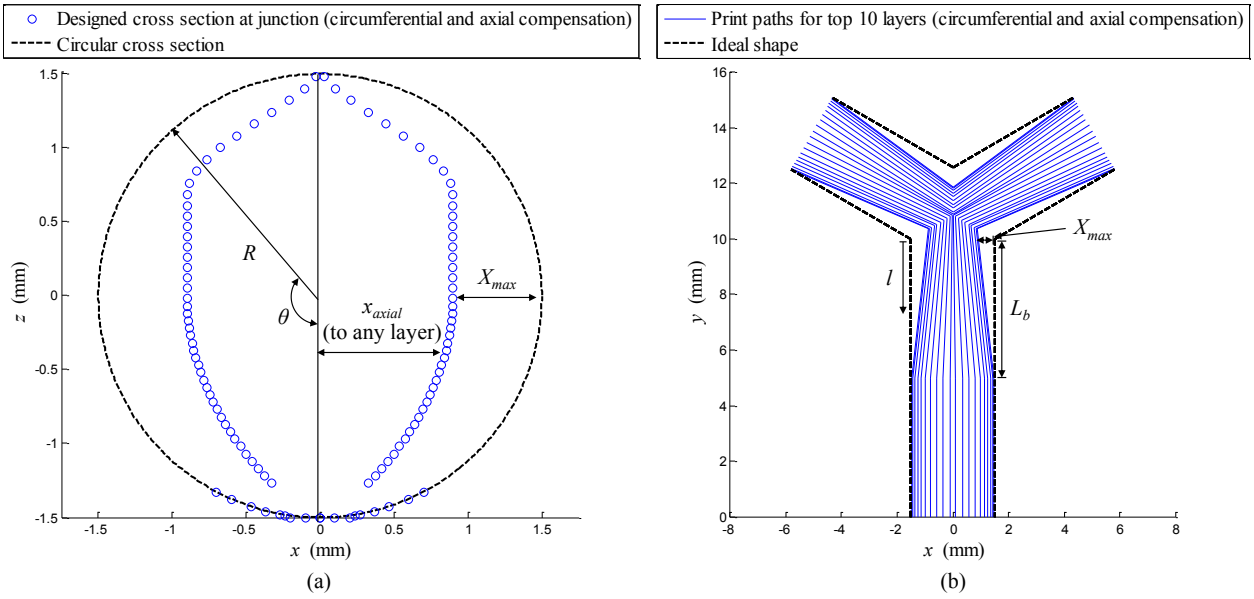

Fig. 8. (a) Designed cross section or compensated printing path at the junction (l = 0) with layer locations indicated in blue after incorporating circumferential and axial deformation compensation, and (b) projected printing paths incorporating the proposed compensation approaches.

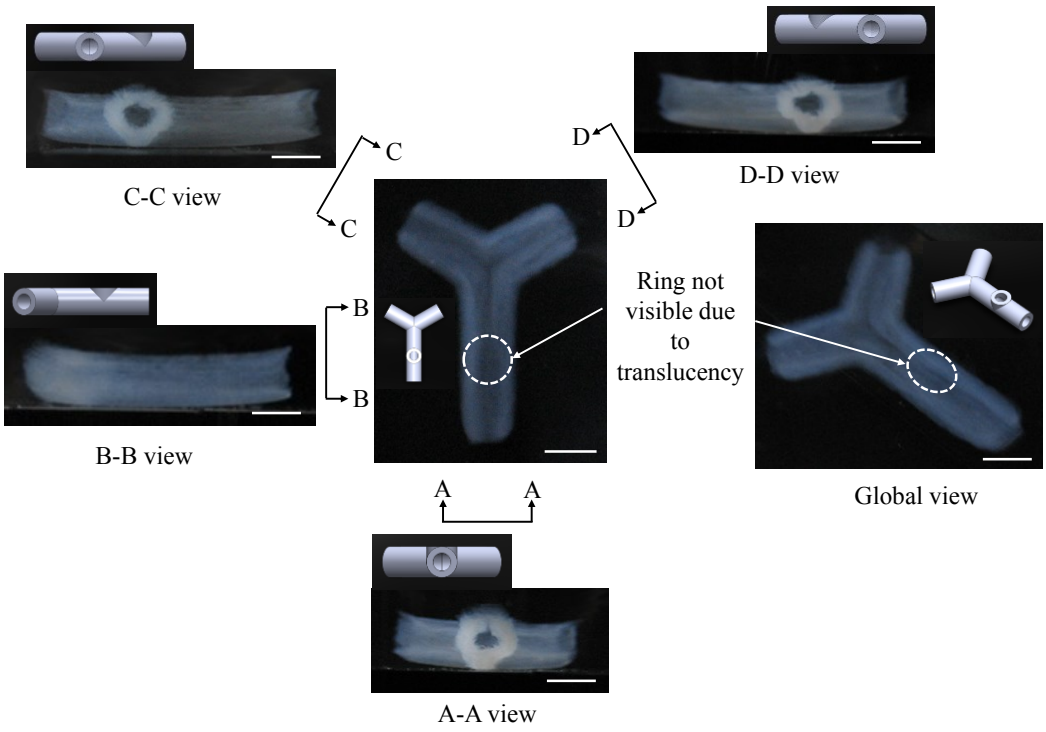

Fig. 9. Horizontal branching tubular structure printed after the incorporation of circumferential and axial deformation compensation (scale bars: 3 mm).

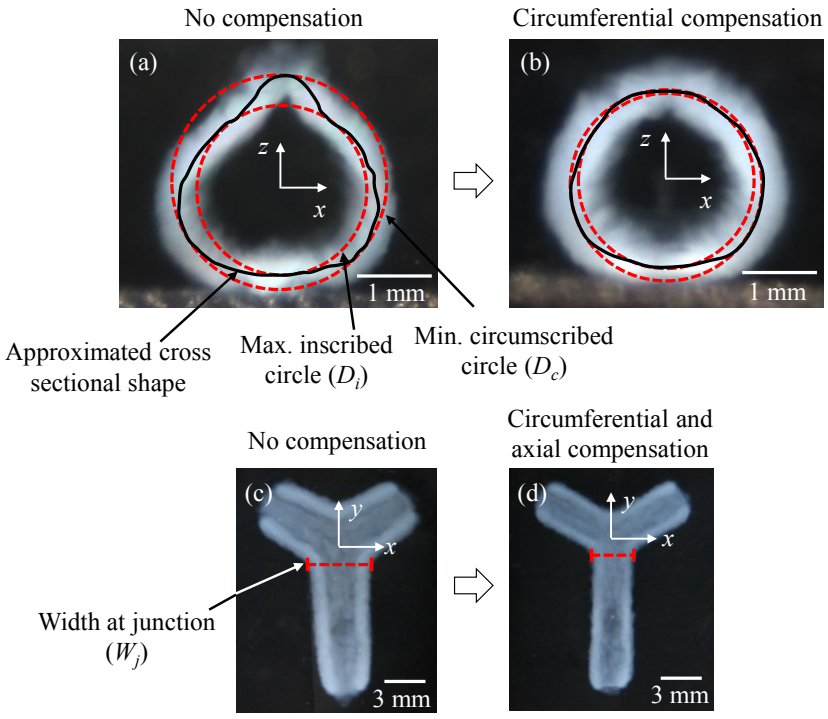

Fig. 10. Roundness R and width ratio W metrics for the evaluation of (a, b) circumferential compensation and (c, d) axial compensation results, respectively.